American Mineralogist, Volume 91, pages 278–284, 2006

Quantitative polarized infrared analysis of trace OH in populations of randomly oriented mineral grains

PAUL D. ASIMOW,* LEO C. STEIN, JED L. MOSENFELDER, AND GEORGE R. ROSSMAN

Division of Geological and Planetary Sciences 170-25, California Institute of Technology, Pasadena, California 91125, U.S.A.

ABSTRACT

Use of infrared spectroscopy as an accurate, quantitative method to measure concentrations of hydrous species in minerals requires consideration of the interactions of anisotropic crystals with infrared light. Ensuring that contributions are identified from species at all orientations in the crystal requires combining three measurements, taken with the electric field polarized along three mutually perpendicular directions. This is typically accomplished by determining the orientation of a crystal in advance, and then sectioning it perpendicular to its principal axes. In many instances, however, natural or experimental samples are not suitable for such handling. Here we demonstrate a method that instead uses at least three randomly sectioned grains, considered to be multiple samples of a homogeneous population. We explain the theory whereby: (1) the orientations of the polarization vectors of measurements taken on these grains are determined by comparison to oriented standards of the same mineral, and (2) the principal-axis spectra of the sample are synthesized from the randomly oriented spectra. By comparison to complementary electron backscatter diffraction (EBSD) data, we demonstrate that determination of orientations using the silicate overtone bands in Fourier-Transform infrared (FTIR) spectra is accurate and precise, with typical angular errors of 6°. We show that this precision is sufficient for the synthetic principal-axis spectra to be essentially indistinguishable from X-ray oriented standard spectra. We demonstrate the application of this technique to determining the OH concentrations in a population of hydrated olivine grains recovered from a high-pressure, high-temperature multi-anvil experiment.

INTRODUCTION

Growing recognition of the critical role of water in chemical and dynamic processes in the Earth has spurred efforts to accurately quantify trace hydrogen concentrations—on the order of 1000 ppm H_2O or less—in nominally anhydrous minerals (NAMs). Promising analytical techniques for achieving this goal include hydrogen manometry, nuclear reaction analysis (NRA), secondary ion mass spectrometry (SIMS), nuclear magnetic resonance (NMR) spectroscopy, and Fourier-transform infrared (FTIR) spectroscopy. Each of these methods has its advantages and disadvantages. Hydrogen manometry has been successfully used to calibrate FTIR spectroscopy (Bell et al. 1995) but, until recently (O'Leary et al. 2004), has required too much sample quantity to be a routine operational technique for the great majority of specimens of interest. NRA has also been used successfully for calibration purposes (Bell et al. 2004, 2003; Hammer et al. 1996; Maldener et al. 2001; Rossman et al. 1988), and has a very low detection limit. It requires special sample preparation, handling, and access to large accelerator facilities, which at the present time are not available for this application. SIMS offers the finest-scale spatial resolution of all these techniques, but requires careful attention to sample preparation and vacuum quality to reduce background hydrogen to a reasonable value (Koga et al. 2003; Kurosawa et al. 1992). Consequently, this method has only been successfully used in a few laboratories. NMR offers the advantage of straightforward, absolute quantification, because the measured ^1H signal is directly proportional to the amount of hydrogen in the sample (Cho and Rossman 1993; Johnson and Rossman 2003; Kohn 1996). However, the necessity to employ powdered samples accentuates problems with adsorbed water that interfere with analysis (Keppler and Rauch 2000), and virtually precludes meaningful determination of fine-scale heterogeneities in OH concentration.

The most widely used technique for measuring trace OH contents in NAMs is FTIR spectroscopy, which provides high precision (depending on sample thickness and OH concentration) and spatial resolution very much like SIMS. Moreover, polarized FTIR measurements can provide information on speciation and bond orientation that cannot be gained using the other techniques. However, FTIR is a relative technique that depends on calibration using other methods, and, until recently, reliable calibrations for many minerals have been lacking. The widely used calibration of Paterson (1982) has been shown to be inaccurate when applied to many minerals, including olivine, garnets, and pyroxenes (Bell et al. 1995, 2003). A more recent calibration for OH in minerals by Libowitzky and Rossman (1997) does not vary much from Paterson's calibration and suffers from the same inherent problem of extrapolation from high to low concentrations. Another major problem concerns the common practice of using unpolarized light in investigations of anisotropic minerals (e.g., Jamtveit et al. 2001; Kohlstedt et al. 1996; Mosenfelder 2000). This introduces nonsystematic errors into analysis (Libowitzky and Rossman 1996), even when samples are consistently oriented with respect

* E-mail: asimow@gps.caltech.edu

0003-004X/06/0203–278$05.00/DOI: 10.2138/am.2006.1937

to the IR beam (Bell et al. 2003).

Even with the advent of updated calibrations and the availability of high-quality polarizers, a major barrier to the practical application of polarized FTIR is the difficulty of properly orienting fine-grained materials, such as experimentally retrieved samples or fine-grained phenocrysts (Jamtveit et al. 2001). One time-consuming approach entails mounting many grains from a sample in random orientations and relying on fortuitous orientation of at least a few grains (Peslier et al. 2002); however, most of the sample yields no useful data in this approach. Herein we provide a new method for analyzing fine-grained samples by correcting polarized spectra obtained on multiple, randomly oriented grains; principal orientations are not needed. This method relies on the assumption that hydrogen concentrations are uniform in all measured grains. We demonstrate the validity of this assumption below in tests of the technique performed on experimentally hydrated olivine crystals. Our technique hinges on comparison of polarized absorbance spectra of X-ray oriented standards to unknowns in the range from ~1500 to 2200 cm^{-1}. This region corresponds to the second-order overtone vibration range in silicate structures; the bands are diagnostic of orientation for a given mineral and independent of OH content. The orientation dependence of this region in both polarized and unpolarized spectra of olivine has been discussed by several previous workers (Jamtveit et al. 2001; Lemaire et al. 2004; Matveev et al. 2005); this paper extends previous work by using the quantitative theory of Libowitzky and Rossman (1996) to handle non-principal spectra. The technique can also be easily adapted for use with spectra taken in reflectance, or in some cases with other techniques such as Raman spectroscopy. At each wavelength, there exists a symmetrical angular distribution of absorbance in crystalline materials (Libowitzky and Rossman 1996) with at most three independent components. Hence the population of spectra can be recombined with the appropriate mathematical transform to synthesize the three principal-axis spectra (**E**-vector parallel to the three principal optical directions) over the entire measured wavelength range. Finally, these synthesized spectra are used for determination of hydrogen content using the recently introduced calibration of Bell et al. (2003), which requires integration of band intensities for polarized spectra in three orthogonal directions. Present versions of software (source code in C and executables for Windows, MacOS, and Linux) for performing all these operations are posted as supplemental online material[1] and updates will be made available through http://minerals.gps.caltech.edu.

[1] Deposit item AM-05-005, Table 1 and software used to perform the calculations in the paper and the authors are making it available in open-source and compiled forms, including compiled executables for macos, linux, and windows; source code, example files, and a README file. Deposit items are available two ways: For a paper copy contact the Business Office of the Mineralogical Society of America (see inside front cover of recent issue) for price information. For an electronic copy visit the MSA web site at http://www.minsocam.org, go to the American Mineralogist Contents, find the table of contents for the specific volume/issue wanted, and then click on the deposit link there.

Mathematical description of the technique

Forward calculation

The basis for synthesizing spectra with the **E**-vector of the incident light polarized in any crystallographic direction derives from the elementary observation of the intensity of light passed by two perfect polarizers rotated by angle ζ relative to one another. The fractional transmission is

$$T(\zeta) = \cos^2 \zeta \tag{1}$$

(Libowitzky and Rossman 1996). The counter-intuitive second power results from light intensity being in units of energy flux; the *amplitude* of the electric and magnetic field oscillations follows the cosine dependence expected from the ordinary vector dot product, but intensity is proportional to the square of amplitude.

Now suppose that at some wavelength λ, there is transmission of light $T_a(\lambda)$ by a crystalline sample when the **E**-vector is polarized parallel to the crystallographic **a**-axis (this orientation is referred to below as **E** ∥ **a**). At this wavelength, the sample is acting like an imperfect polarizer with partial extinction parallel to the *a*-axis. It follows that, as the **E** vector rotates away from the **a**-axis through angle ζ, this component of transmission behaves as

$$T(\zeta,\lambda) = T_a(\lambda)\cos^2 \zeta\,. \tag{2}$$

Now, let us introduce the (θ, φ) coordinate system shown in Figure 1. If $T_b(\lambda)$ is transmission by a sample when the **E** vector

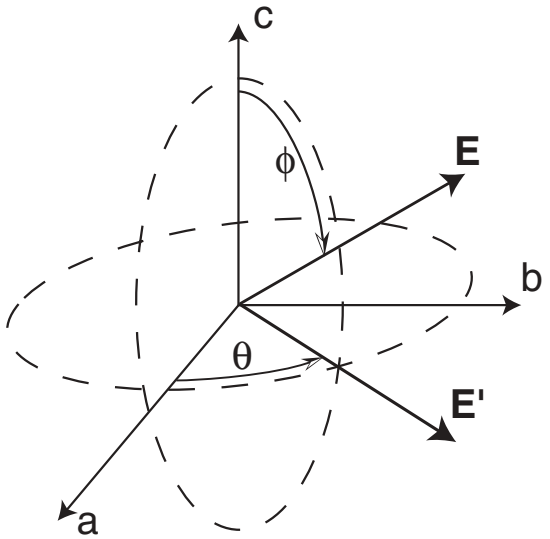

Figure 1. The coordinate system in which the orientation of the polarization vector **E** of FTIR measurement is expressed, relative to the **a**, **b**, and **c** axes of an orthorhombic crystal. Vector **E'** is the projection of **E** onto the (**a**-**b**) plane. Angle θ is the azimuth of **E'** in the (**a**-**b**) plane, measured from the **a**-axis, and φ is the angle between **E** and the c-axis. By convention, both θ and φ are reported in the domain 0 to 90°, as the optical properties are symmetrical with respect to reflection about the (**a**-**b**), (**b**-**c**), and (**a**-**c**) planes.

is polarized in the **b** direction, it follows by superposition and Equation 2 that transmission along the direction given by projecting the **E** vector into the (**a-b**) plane (**E'** in Fig. 1) is

$$T_\theta(\theta,\lambda) = T_a(\lambda)\cos^2\theta + T_b(\lambda)\sin^2\theta\,. \quad (3)$$

Then, if $T_c(\lambda)$ is transmission by the sample when the **E** vector is parallel to the **c** direction, the same operation, applied in the plane that contains the **c**-axis, the polarization vector, and the **E'** direction, leads to

$$T(\theta,\phi,\lambda) = T_c(\lambda)\cos^2\phi + T_\theta(\theta,\lambda)\sin^2\phi\,. \quad (4)$$

Application of Equations 3 and 4 in sequence leads to

$$T(\theta,\phi,\lambda) = T_a(\lambda)\cos^2\theta\sin^2\phi + T_b(\lambda)\sin^2\theta\sin^2\phi + T_c(\lambda)\cos^2\phi. \quad (5)$$

This result allows calculation of the transmission spectrum of a sample or standard with arbitrary crystallographic orientation relative to the **E** vector, if the three principal axis spectra are known.

Another counter-intuitive aspect of transmission spectra taken in non-principal directions is the dependence of the measured spectrum on sample thickness. When expressed in absorbance units, i.e.,

$$A(\lambda) = -\log[T(\lambda)] \quad (6)$$

spectra taken in principal directions scale linearly with sample thickness. That is, at each wavelength they obey the Beer-Lambert law, and thus the entire spectrum obeys this law. Transmission, however, varies exponentially rather than linearly with thickness. Because Equation 5 is a linear superposition of transmissions rather than absorbances, we find that spectra in non-principal directions do not obey the Beer-Lambert law and that different absorbers may have different relative strength in non-principal axis spectra taken at different thicknesses (Libowitzky and Rossman 1996). To deal with this problem, it is important that the principal axis spectra be scaled to the measured thickness before Equation 5 is applied; the reverse order of operations is not equivalent. Hence, if the standard spectra are normalized (e.g., to 1 mm thickness) and d is the thickness of interest expressed in the normalized units (e.g., mm), we have:

$$T(d,\theta,\phi,\lambda) = [T_a(\lambda)]^d \cos^2\theta\sin^2\phi + [T_b(\lambda)]^d \sin^2\theta\sin^2\phi + [T_c(\lambda)]^d \cos^2\phi. \quad (7)$$

Note that, except for the cases where two of the terms on the right-hand side of Equation 7 are zero, this is not equal to raising the entire right-hand side of Equation 5 to the d power, which would be consistent with the Beer-Lambert law.

Inverse calculation

We do not have a direct, closed-form solution for determining the orientation of a measured polarization vector. Therefore, we proceed to search the orientation space (θ, φ) for the best-fitting direction, in the sense that known standard spectra taken in the **a**, **b**, and **c** directions, combined using Equation 7, produce the best match to the observed spectrum over some reference wavelength range. In the present case, we use the silicate overtone region at 1500 to 2200 cm^{-1}. For this search, we use a modified Newton's method implemented by the *dfpmin* algorithm of Press et al. (1992). This requires definition of an error function to be minimized and the partial derivatives of the error function with respect to all the optimization variables. In practice, we find that the best way to fit the orientations, with minimum sensitivity to noise and background subtraction errors, is to minimize the misfit between the first derivatives of the unknown and synthetic spectra. Furthermore, we allow for the possibility that the thickness of the unknown grain was measured incorrectly and, optionally, include the unknown grain thickness as an additional fitting parameter. Hence, for a spectrum defined by a series of data points at discrete values of wavelength λ and normalized **a**, **b**, and **c**-axis standards either measured or interpolated to the same set of wavelength values, the error function is

$$Err(d,\theta,\phi) = \sum_\lambda \left[\frac{dT^{\text{unknown}}(\lambda)}{d\lambda} - \frac{dT^{\text{std}}(d,\theta,\phi,\lambda)}{d\lambda}\right]^2. \quad (8)$$

In practice, the spectral derivatives are taken on data smoothed with a nine-sample moving average; this is less sensitive to noise than the derivative of the raw spectra. The partial derivatives of this expression in the d, θ, and φ directions can be readily obtained. The search is found to converge readily to a unique solution in most cases; to check against local minima, the search is restarted several times from different initial guesses.

Synthesis of population-mean principal-axis spectra

Given a set of at least three spectra with non-coplanar polarization vectors and equal sample thickness, the synthesis of principal-axis spectra is a linear least-squares problem when expressed in transmission units, once the orientation of the measurements is determined. In the examples shown below, we use the orientations determined by fitting the FTIR spectra in the silicate overtone region, relative to X-ray oriented standards of the same mineral. However, the synthesis step can be performed equally well with orientations determined by any method. In particular, EBSD data are more precise, require only a crystal definition file, and do not require FTIR spectra of oriented standards. If orientations are available from a more precise technique, they should be used, but we emphasize that they are not necessary—the entire analysis can be done with FTIR data alone.

Generally, a set of $2n$ spectra is obtained from n grains with two extinction directions each. The orientation of the polarization vector of each measurement relative to the crystal axes is determined as described above. Although thickness errors are allowed in orientation fitting, for the simple linear synthesis operation described here all the unknowns must have approximately the same thickness; differences of up to ~10% should be negligible. A non-linear synthesis operation combining spectra taken at widely different thicknesses could readily be implemented, but the simplicity of the linear solution is appealing and easily understood so we present it here. At constant d, Equation 7 is a linear combination of the transmissions along the principal directions at each wavelength. For $n \geq 2$, the $2n$ statements of Equation 7 constitute an over-constrained linear least-squares

problem. The solution vector $(T_a, T_b, T_c)(\lambda)$ is obtained by singular value decomposition (Press et al. 1992) for every wavelength of interest, assembled into principal-axis spectra, converted back to absorbance units, and finally normalized (note that the synthetic principal-axis spectra do obey the Beer-Lambert law, and can be normalized in the usual manner). The synthesized principal-axis absorbance spectra are then ready to be integrated and converted to water contents using the Bell et al. (2003) calibration for olivine or some other mineral-specific or general calibration for other materials.

Experimental methods

The standards used in this study were X-ray oriented crystals of San Carlos olivine (Miller et al. 1987). Polarized transmission spectra were collected for the standard olivine, and are shown below. We use transmission FTIR spectra for orientation determinations in this paper, but we note that Raman spectra are also sensitive to orientation. Depolarized Raman spectra for the same standards are available at http://minerals.gps.caltech.edu. For Raman spectra taken without a depolarizer, the absolute peak heights cannot be used for quantitative purposes (cf. Arredondo and Rossman 2002). However, the presence or absence of the two peaks at 882 and 919 cm^{-1} has been found sufficient to distinguish between the three optical orientations of olivine; both peaks are present when the crystallographic orientation does not correspond to one of the optical directions.

Two sets of "unknowns" were used to test the orientation and synthesis techniques. The first set consisted of 27 randomly oriented fragments of a single crystal of San Carlos olivine. These were set in an epoxy disk, polished on one side, sliced, and then polished on the other side, yielding a thick section used for both EBSD and FTIR. Thicknesses of individual grains in this mount ranged from 163 to 275 µm. The other unknown was a 160 µm thick section of a sample retrieved from a 24 h multi-anvil experiment at 8 GPa and 1150 °C, in which 15 spectra from 8 grains of hydrated San Carlos olivine crystals were measured. The full details of this and other experiments analyzed in the manner developed here are given in a separate paper (Mosenfelder et al. 2006, this issue).

Electron backscatter diffraction (EBSD) was used to determine precisely the orientations of the dry olivine fragments. The sample was given a very thin carbon coat (~3 nm) and EBSD patterns were collected using a LEO 1550VP field emission SEM operating at 15 kV with a 60 µm aperture in high-current mode. At least three EBSD patterns were retrieved from each of 27 fragments. The patterns were indexed using a crystal definition file for $(Mg_{0.9},Fe_{0.1})_2SiO_4$ olivine based on the X-ray refinement of McCormick et al. (1987). HKL software was used for collection and reduction of the patterns. The angular standard deviation of multiple determinations on a given fragment was about 1°. The **z** direction of the SEM coordinate system was normal to the sample mount, and the **x** direction was fixed by rotating the sample until a fiducial mark was parallel to the **x**-coordinate of the SEM stage. The result is a mean set of Euler angles (φ_1, Φ, φ_2) describing the orientation of the crystal axes of each olivine grain relative to the (**x**, **y**, **z**) reference frame of the SEM. The sample mount was then transferred to the FTIR microscope with the fiducial mark parallel to the 0° direction on the microscope stage.

A Nicolet Magna 860 FTIR spectrometer was used for all the IR measurements. All spectra were collected using the attached Spectra-Tech Continuµm microscope. Spectra were acquired in both of the two perpendicular extinction directions of each crystal. For the dry olivine fragments, the stage rotation angle of each measured extinction direction was noted. Together with the EBSD measurement, this angle serves to fix the orientation of the polarization vector relative to the crystal axes of the unknown grain (Table 1).[2] Polarized transmission spectra were recorded from 4000 to 650 cm^{-1} by averaging 400 or more scans with 2 cm^{-1} resolution, using a GLOBAR infrared light source, a KBr beamsplitter, a wire-grid on CaF_2 polarizer, and an MCT-A detector. We used square apertures from 50 to 100 µm in width to collect spectra from regions as free as possible from cracks and grain boundaries. Polychlorotriflouroethylene oil was used to eliminate interference fringes in spectra taken on the standards. Some spectra from the hydrated olivine experiment showed evidence for contamination by organic materials from epoxy or other mounting polymers, most obviously in the range from ~2800–3000 cm^{-1}. Spectra of the pure epoxy we used showed that there are also sharp peaks in the silicate overtone region. To deal with this problem, we subtracted the organic peaks from the sample spectrum and also modified the orientation-fitting algorithm to ignore the spectral regions contaminated by these organic peaks.

We wrote a new background subtraction program to support this effort. Existing background subtraction methods were found inadequate for one or more of the tasks at hand. Inconsistent subtraction under the broad region of silicate overtone bands, which sit on the shoulder of a very large absorbance at wavenumbers less than ~1100 cm^{-1}, leads to orientation errors. Poor or inconsistent subtraction under the OH-stretching region leads directly to errors in estimated OH contents. Epoxy-related peaks overlapping the OH-stretch region need to be removed. The assumption underlying the method is that background signals are generally concave-upward (in absorbance), whereas concave-downward regions indicate peaks. The algorithm begins by taking a 15-point moving average to filter out interference fringes that are often seen in thin samples. It then automatically finds a specified number (typically 100) of "anchor points" by sequentially adding whichever point on the spectrum is farthest below a piecewise linear fit through the anchors already found (beginning with a line between a point high on the 1100 cm^{-1} feature and a point in the featureless region near 4000 cm^{-1}). Regions containing anomalous negative features (e.g., bands attributed to CO_2 in the path of the beam, which can vary between the background and sample spectrum) can be excluded from the anchor selection process. The user can specify anchor points manually to account for broad concave-down features that are judged to be features of the background rather than signal. The piecewise linear fit is then replaced by a cubic spline through the anchor points, except in intervals where the user flags the program to retain the linear form. Finally, regions with extraneous positive or negative features, e.g., epoxy peaks, can be removed and replaced with linear segments in the subtracted spectrum. The background subtraction software is fully documented and included in the supplemental online material and maintained at http://minerals.gps.caltech.edu.

Results

Precision and accuracy of orientation determination

The random fragments of San Carlos olivine were used to assess the capability of the FTIR technique to recover the known orientations determined by EBSD. The results are shown in Figure 2 (and Supplementary Online Table 1). The pole figure in Figure 2a compares the corresponding polarization vector determinations by the two methods. We note that most of the measured extinction directions are close to the boundaries of the octant; this may be a selection effect resulting from the moderate cleavage of olivine during crushing. However, there are some intermediate directions in the population. The maximum error found, expressed as the angle between the polarization vectors determined by the EBSD and FTIR methods, is 12.7°. The mean error is 6.2°. The caption to Figure 2 explains the range of possible errors that could be obtained in the coordinate system used, and Figure 2b shows that the actual errors are much smaller than would be expected from a random distribution; hence, we are able to recover useful orientation information from the silicate overtone region of the FTIR spectrum. Whether the precision of this determination is adequate depends on the purpose for which the orientations are being determined. The FTIR method is not as precise as EBSD or X-ray diffraction. It is similar to examination of optical interference figures or Raman spectra for sections that are close to principal orientation and considerably better for intermediate orientations. We demonstrate below that the precision of determinations based on the silicate overtone peaks is sufficient to perform the synthesis of principal-axis spectra in the silicate overtone region and recover spectra nearly indistinguishable from the X-ray oriented standards. The angular sensitivity of absorbance varies systematically with the absolute absorbance; stronger bands are more sharply restricted to orientations near principal axes (Libowitzky and Rossman 1996). Hence the integrated absorbance of the OH-stretching bands will have sensitivity to orientation errors similar

[2] See footnote page 279.

to or smaller than the silicate overtone bands if their maximum absorbance is similar to or smaller than that of the silicate overtone bands. Thus, for samples with maximum absorbance in the OH-region less than or equal to the absorbances in the silicate overtone region, successful recovery of the principal-axis silicate overtone spectra demonstrates that the precision is also sufficient to perform the synthesis in the OH-stretch region and to determine OH contents.

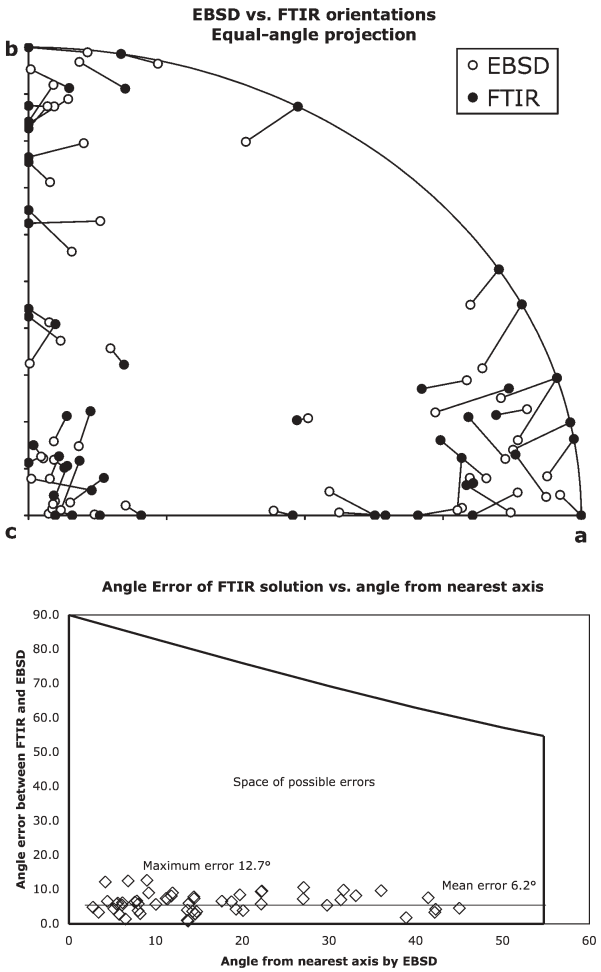

FIGURE 2. Performance of the FTIR orientation method, relative to EBSD determinations, for randomly oriented fragments of San Carlos olivine (see Table 1). (top) A stereographic equal-angle projection of the positive octant of the crystallographic coordinate system showing the orientation of measured polarization vectors according to EBSD (open circles) compared to the best-fitting orientation determined from the silicate overtone region of the FTIR spectrum (filled circles). Corresponding determinations by the two methods are connected by lines. (bottom) The angular error in the FTIR determination is plotted against the angle between the **E**-vector and the nearest crystallographic axis, to show that the method works for intermediate directions as well as near principal axes. The angle from the nearest axis is in the range 0 to 54.7° and the maximum error ranges from 90° when the E-vector is parallel to an axis to 54.7° when the **E**-vector is along the (111) direction. Random orientation solutions would populate the possible error range evenly. The orientation determinations are clearly not random and their quality is independent of distance from the nearest axis.

Synthesis of principal axis spectra

Comparison to standard spectra. From the 54 spectra on randomly oriented fragments of San Carlos olivine, using orientations determined by fitting the FTIR spectra, we synthesized three principal-axis spectra. In Figure 3, these are shown and compared to the principal-axis spectra taken on X-ray oriented standard grains from the same locality. This is not a circular exercise. If the silicate overtone spectra of olivine were not highly reproducible or if our model of the orientation-dependence of the spectra were incorrect, we could have recovered principal-axis spectra that do not resemble the standard spectra.

We repeated the same exercise with 15 spectra determined from eight olivine grains from the multi-anvil hydration experiment. In this case the orientations are not independently known and, although the starting material is again San Carlos olivine, it has been subjected to considerable processing (equilibration with water and quenching of defect populations from high pressure and temperature) that might, in principle, affect its infrared spectrum. However, apart from some small extra peaks attributable to epoxy contamination, the recovery of the principal-axis silicate overtone spectra is excellent (Fig. 3).

The match between the principal-axis silicate overtone spectra

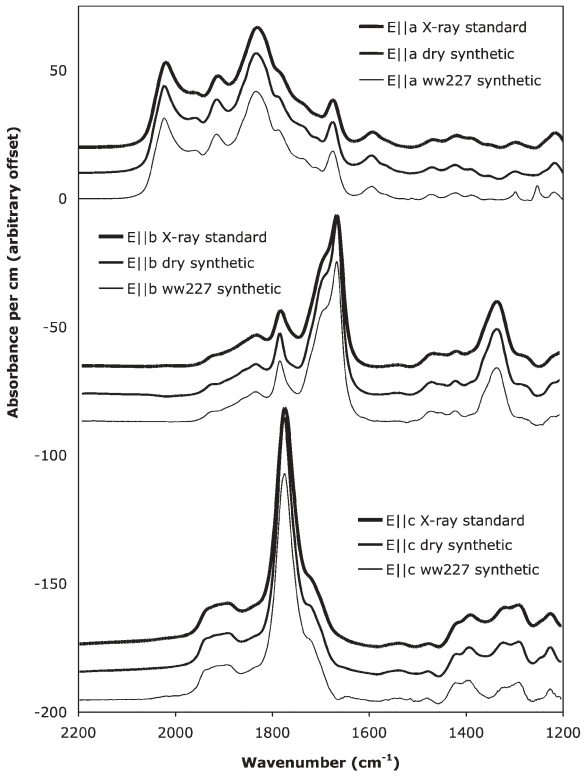

FIGURE 3. Comparison of silicate overtone region of the FTIR spectra for X-ray oriented San Carlos olivine standards (sample GRR997, heavy lines) to the principal-axis spectra synthesized from 54 measurements on randomly oriented fragments of a single olivine from the same locality (medium lines) and from 15 measurements of randomly oriented olivines hydrated at 8 GPa and 1150 °C (light lines). Spectra are normalized to 1 cm sample thickness and offset for clarity. The recovered principal-axis spectra match the standard spectra quite well.

taken on X-ray oriented standards and those synthesized from randomly oriented grains, dry or hydrated, demonstrates that our theory for the orientation dependence of FTIR spectra is at least approximately correct and that in practice the orientation determinations are sufficiently accurate to allow the synthesis procedure.

OH-stretching region. Figure 4 shows the OH-stretching region of 15 spectra collected from grains in the multi-anvil olivine hydration experiment together with the principal-axis spectra synthesized from these data, using orientations determined from the silicate overtone region of the same spectra. Within error (±5% random errors, see below), all of the spectra plot within the envelope defined by the synthetic **E** ∥ **a** (maximum absorbance) and **E** ∥ **b** (minimum absorbance) spectra. This plot shows the advantage of using all the data available with the current technique, as opposed to choosing a representative spectrum thought to be close to each principal direction. Spectrum 22, for example, is found to be oriented 29.4° away from the **a**-axis, but qualitatively looks similar to an **E** ∥ **a** spectrum. If this spectrum were chosen as the **E** ∥ **a** sample, the resulting water content would be too low by 11%. On the other hand, the spectrum predicted using the synthesized principal-axis spectra and the determined orientation of this measurement predicts the integral of this spectrum to within 1%. Likewise, spectrum 33 resembles an **E** ∥ c spectrum, but is found to be 30° away from the **c**-axis. Its integral is 14% higher than the true **c**-axis spectrum, and had it been chosen as the representative **c**-axis sample, a significant fraction of the **a**-axis absorption would have been over-counted.

Integration of the three synthesized principal axis spectra between 2950 and 3750 cm^{-1} and application of the integral extinction coefficient of 0.188 ± 0.012 ppm H_2O/cm^2 from Bell et al. (2003) yields a water content of 2100 ± 150 ppm H_2O by weight. This value is about 2.5 times larger than the value measured by Kohlstedt et al. (1996) at similar conditions, using the Paterson (1982) calibration. Revision of the water contents in olivines saturated at high pressure is discussed elsewhere (Mosenfelder et al. 2006, this issue). The accuracy of this number is a question of calibration, which introduces an uncertainty of at least the 6% formal uncertainty in the extinction coefficient of Bell et al. (2003). We note that there may be further errors in the application of this extinction coefficient to olivine with different spectral shapes (Bell et al. 2003), but we are unable to quantify these errors at this time. Here, our interest is in the precision of the measurement of integrated absorbance resulting from our new FTIR technique.

The standard deviation of individual determinations relative to the three-component model is 6.7% (Fig. 5). A total water content derived from adding three such measurements would have a standard error of 11.7%. On the other hand, combining 15 such measurements to constrain the model, as in this case, reduces the standard error of the mean of three-point trials to ±3%. Furthermore we find that, in practice, the differences in estimated water contents resulting from different operators performing the steps described above (background subtraction, orientation fitting with or without consideration of thickness errors and with

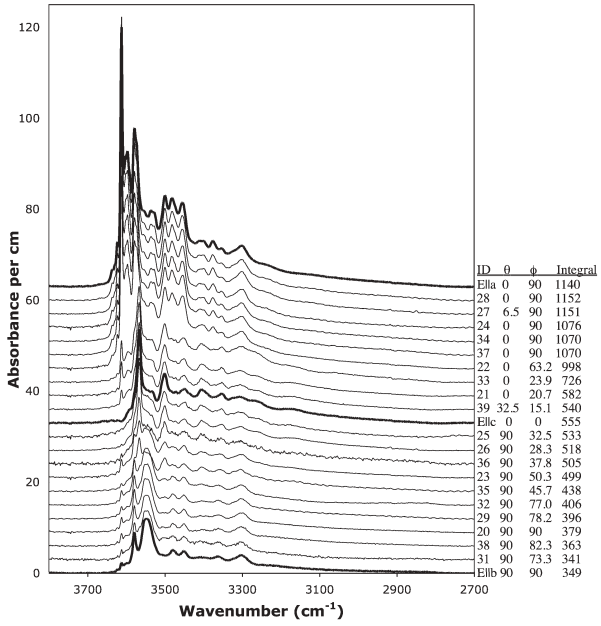

FIGURE 4. The OH-stretching region of 15 FTIR spectra on randomly oriented olivine grains from a multi-anvil hydration experiment and the principal-axis spectra synthesized from these data (bold lines). The table at right gives the fitted or assumed orientation (θ, φ) in the coordinate system of Figure 1 and the apparent H_2O content (in ppm) from the integral of each spectrum (Bell et al. 2003). Spectra are normalized to 1 cm thickness and offset for clarity.

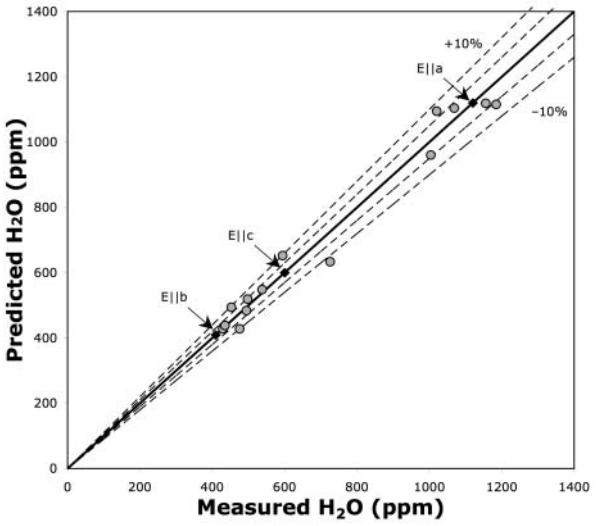

FIGURE 5. An estimate of the improvement in precision resulting from the use of all available grains is derived by comparing the H_2O content converted from the integral of each individual spectrum in the olivine hydration experiment with the value predicted from the orientation of the spectrum and the best-fitting synthesized principal-axis spectra. The measured value is plotted against the prediction for each spectrum; the 1:1 line as well as ±5% and ±10% error contours are shown. The black diamonds show the model principal axis values summed to obtain the best-estimate water content. The gray circles show the 15 independent determinations used to constrain the fit.

or without subtraction of epoxy peaks, etc.) are 2% except for samples with difficult background contamination issues and/or very low structural water contents. Hence, we feel that application of the present technique to populations of multiple spectra reduces operational and random errors to a level comparable to the formal uncertainty in the calibration. This is the highest precision that is likely to be meaningful: higher precision on integrated absorbance will not give higher precision on actual H_2O content because of limitations in the calibration. For this experiment, our final estimate of the errors, both random and systematic, is 7%, and is dominated by the calibration uncertainty.

The technique described herein makes it possible to use FTIR spectra from all measurable grains in a population as constraints on water content with no additional sample preparation effort; as more data are included, the uncertainty in the mean water content decreases. This technique can be extended to minerals in any crystal system. The synthesis of principal spectra can be done either with the orientations determined by FTIR, as shown here, or using independent orientation data such as EBSD. In the latter case, oriented standards are not required.

ACKNOWLEDGMENTS

This work was supported by the National Science Foundation through grant OCE-0241716 to P.D.A. and EAR-0337816 to G.R.R. and by the Caltech SURF program. Thanks to Scott Sitzman of HKL technology for EBSD advice. The manuscript was improved by comments from Eugen Libowitzky, an anonymous reviewer, and associate editor Alison Pawley.

REFERENCES CITED

Arredondo, E.H. and Rossman, G.R. (2002) Feasibility of determining the quantitative OH content of garnets with Raman spectroscopy. American Mineralogist, 87, 307–311.

Bell, D., Rossman, G.R., Maldener, J., Endisch, D., and Rauch, F. (2004) Hydroxide in kyanite: a quantitative determination of the absolute amount and calibration of the IR spectrum. American Mineralogist, 89, 998–1003.

Bell, D.R., Ihinger, P.D., and Rossman, G.R. (1995) Quantitative analysis of trace OH in garnet and pyroxenes. American Mineralogist, 80, 465–474.

Bell, D.R., Rossman, G.R., Maldener, J., Endisch, D., and Rauch, F. (2003) Hydroxide in olivine: a quantitative determination of the absolute amount and calibration of the IR spectrum. Journal of Geophysical Research, 108(2105), DOI: 10.1029/2001JB000679.

Cho, H. and Rossman, G.R. (1993) Single-crystal NMR studies of low-concentration hydrous species in minerals: grossular garnet. American Mineralogist, 78, 1149–1164.

Hammer, V.M.F., Beran, A., Endisch, D., and Rauch, F. (1996) OH concentrations in natural titanites determined by FTIR spectroscopy and nuclear reaction analysis. European Journal of Mineralogy, 8, 281–288.

Jamtveit, B., Brooker, R., Brooks, K., Larsen, L.M., and Pedersen, T. (2001) The water content of olivines from the North Atlantic Volcanic Province. Earth and Planetary Science Letters, 186(3–4), 401–415.

Johnson, E.A. and Rossman, G.R. (2003) The concentration and speciation of hydrogen in feldspars using FTIR and ^{1}H MAS NMR spectroscopy. American Mineralogist, 88, 901–911.

Keppler, H. and Rauch, M. (2000) Water solubility in nominally anhydrous minerals measured by FTIR and ^{1}H MAS NMR: the effect of sample preparation. Physics and Chemistry of Minerals, 27, 371–376.

Koga, K., Hauri, E., Hirschmann, M., and Bell, D. (2003) Hydrogen concentration analyses using SIMS and FTIR: comparison and calibration for nominally anhydrous minerals. Geochemistry, Geophysics, and Geosystems, 4, DOI: 10.1029/2002GC000378.

Kohlstedt, D.L., Keppler, H., and Rubie, D.C. (1996) Solubility of water in the α, β, and γ phases of $(Mg, Fe)_2SiO_4$. Contributions to Mineralogy and Petrology, 123, 345–357.

Kohn, S.C. (1996) Solubility of H_2O in nominally anhydrous mantle minerals using ^{1}H MAS NMR. American Mineralogist, 81, 1523–1526.

Kurosawa, M., Yurimoto, H., Matsumoto, K., and Sueno, S. (1992) Hydrogen analysis of mantle olivine by secondary ion mass spectrometry. In Y. Syono and M.H. Manghnani, Eds., High-pressure research: application to Earth and planetary sciences, p. 283–287. American Geophysical Union, Washington, D.C.

Lemaire, C., Kohn, S.C., and Brooker, R.A. (2004) The effect of silica activity on the incorporation mechanisms of water in synthetic forsterite: a polarised infrared spectroscopic study. Contributions to Mineralogy and Petrology, 147, 48–57.

Libowitzky, E. and Rossman, G.R. (1996) Principles of quantitative absorbance measurements in anisotropic crystals. Physics and Chemistry of Minerals, 23(6), 319–327.

——— (1997) An IR absorption calibration for water in minerals. American Mineralogist, 82, 1111–1115.

Maldener, J., Rauch, F., Gavranic, M., and Beran, A. (2001) OH absorption coefficients of rutile and cassiterite deduced from nuclear reaction analysis and FTIR spectroscopy. Mineralogy and Petrology, 71, 21–29.

Matveev, S., Portnyagin, M., Ballhaus, C., Brooker, R., and Geiger, C.A. (2005) FTIR spectrum of phenocryst olivine as an indicator of silica saturation in magmas. Journal of Petrology, 46, 603–614.

McCormick, T.C., Smyth, J.R., and Lofgren, G.E. (1987) Site occupancies of minor elements in synthetic olivines as determined by channeling-enhanced X-ray emission. Physics and Chemistry of Minerals, 14, 368–372.

Miller, G.H., Rossman, G.R., and Harlow, G.E. (1987) The natural occurrence of hydroxide in olivine. Physics and Chemistry of Minerals, 14, 461–472.

Mosenfelder, J.L. (2000) Pressure dependence of hydroxyl solubility in coesite. Physics and Chemistry of Minerals, 27 (9), 610–617.

Mosenfelder, J.L., Deligne, N.I., Asimow, P.D., and Rossman, G.R. (2006) Hydrogen incorporation in olivine from 2–12 GPa. American Mineralogist, 91, 285–294.

O'Leary, J.A., Eiler, J.M., Rossman, G.R., and Wang, Z. (2004) Micro-analysis of absolute water concentration in minerals. EOS Transactions AGU, 85(47 (Fall meeting supplement)), Abstract T41B-1187.

Paterson, M. (1982) The determination of hydroxyl by infrared absorption in quartz, silicate glasses and similar materials. Bulletin de Mineralogie, 105, 20–29.

Peslier, A.H., Luhr, J.F., and Post, J. (2002) Low water content in pyroxenes from spinel-peridotites of the oxidized, sub-arc mantle wedge. Earth and Planetary Science Letters, 201, 69–86.

Press, W.H., Teukolsky, S.A., Vetterling, W.T., and Flannery, B.P. (1992) Numerical recipes in C: the art of scientific computing. Cambridge University Press, U.K.

Rossman, G.R., Rauch, F., Livi, R., Tombrello, T.A., Shi, C.R., and Zhoi, Z.Y. (1988) Nuclear reaction analysis of hydrogen in almandine, pyrope and spessartite garnets. Neues Jahrbuch fur Mineralogie Monatshefte, 4, 172–178.

MANUSCRIPT RECEIVED MARCH 9, 2005
MANUSCRIPT ACCEPTED SEPTEMBER 11, 2005
MANUSCRIPT HANDLED BY ALISON PAWLEY